

High Performance Ge-on-Si Photodetector With Optimized Light Field Distribution by Dual-Injection

Jishi Cui , Hongmin Chen, Jianping Zhou, and Tiantian Li 

Abstract—This paper proposed a photodetector with a dual-injection structure. Input power is splitted into two beams by a 3 dB beam splitter at the incident end and then coupled into the photodetector, which can make the light field distribution in the germanium absorption layer more uniform. With the same active area structure, the responsivity of the dual-injection structure can be increased by 45.73% at 108.33 mW, the saturated optical power could be induced by 44.76%, and the bandwidth can be improved by 6.74 GHz at 20 mW comparing with the single-injection structure. The dual-injection structure improves the performance of the device without increasing the complexity.

Index Terms—Silicon photonics, Ge-on-Si photodetector, dual-injection structure.

I. INTRODUCTION

SILICON photonics has attracted extensive research interest because of the compatibility with CMOS (Complementary Metal-Oxide-Semiconductor) process, easy integration, low cost, compact size, and low power consumption [1]–[5]. It has shown great application value in data center, communication, sensing, high-performance computing and artificial intelligence area [6], [7]. As the key component of the receiver, silicon-based photodetector has significant influence on the performance of the entire transceiver system. Since the absorption limit wavelength of silicon is 1100 nm, the germanium which has similar lattice structure with silicon, compatible with CMOS technology and has a longer absorption wavelength range is mainly used as an absorption material in silicon photonics circuits. In recent years, many works about Ge-on-Si photodetectors have been reported [8]–[13]. For integrated optical systems, high-power and high-speed devices were needed in some fields, such as microwave photonics, receivers in optical communications and optical sensing system [14], [15].

In the traditional single-injection structure, the light field is only distributed in a part of the germanium absorption layer,

Manuscript received November 15, 2021; accepted February 19, 2022. Date of publication February 23, 2022; date of current version March 11, 2022. This work was supported in part by the Natural Science Foundation of Fujian Province, China, under Grant 2021J01600, in part by the Natural Science Foundation of China under Grant 62105260, in part by the State Key Laboratory of Advanced Optical Communication Systems and Networks, China, and in part by the Youth Project of Fujian Provincial Department of Education under Grant JAT200648. (*Corresponding author: Tiantian Li.*)

Jishi Cui, Hongmin Chen, and Jianping Zhou are with the School of Information Engineering, Sanming University, Sanming 365004, China (e-mail: jscui@fjsmu.edu.cn; hongmin_chen@126.com; 20190117@fjsmu.edu.cn).

Tiantian Li is with the School of Electronic Engineering, Xi'an University of Posts and Telecommunications, Xi'an 710121, China (e-mail: tiantianli@xupt.edu.cn).

Digital Object Identifier 10.1109/JPHOT.2022.3153694

and only occupies a small part of the whole germanium layer. The distribution of the light field depends on the transmission characteristics of light in the Si/Ge heterojunction. On one hand, the uneven distribution causes the light field too strong in some areas, which will suffer from the saturation effect more easily. On the other hand, the uneven light field will lead to uneven distribution of photo-generated carriers, which will produce carrier-screening effect [16] and reduce the mean free path of carriers [17].

Here, we proposed a novel photodetector structure with a dual-injection input waveguide.. Benefitted from the more uniform light field distribution, this novel structure can overcome some defects in the traditional single-injection one and shows improved performance.

II. STRUCTURE

Fig. 1 shows the schematic diagram of the designed Ge-on-Si photodetector with single- and dual-injection. All the width of the silicon waveguides is 600 nm, and the width of the silicon substrate for epitaxial germanium as active area is 1.6 μm . The silicon substrate and the silicon waveguide in active area are coupled by the taper structure. Distinguished from the single-injection structure, the waveguide of the dual-injection structure photodetector divides the power of the incident light into two parts by a 3 dB beam splitter before coupling into the active area as indicated in Fig. 1(a). Fig. 1(b) is the three-dimensional view of a dual-injection photodetector. The blue area is silicon, the green one is germanium and the gray one is the aluminum electrode. The thickness of the silicon waveguide and germanium absorption layer are 220 nm and 500 nm respectively. The thickness of the silicon slab area between the silicon waveguide and the electrode is 60 nm with the length of 1.5 μm . The slab area below the electrode region is heavily doped with p-type with a concentration of $1 \times 10^{20} \text{ cm}^{-3}$, and the top layer of germanium is heavily doped with a n-type with a concentration of $1 \times 10^{20} \text{ cm}^{-3}$. The heavy doping is for good ohmic contact. The refractive indices of silicon and germanium are 3.48 and 4.28 respectively, and the absorption coefficient of germanium is 5.67×10^{-3} in our calculation. The incident wavelength λ is 1550 nm for modelling.

III. LIGHT FIELD

The distribution of optical field power (top view) in the germanium absorption layer of the single- and dual-incidence photodetectors calculated by finite difference time domain method

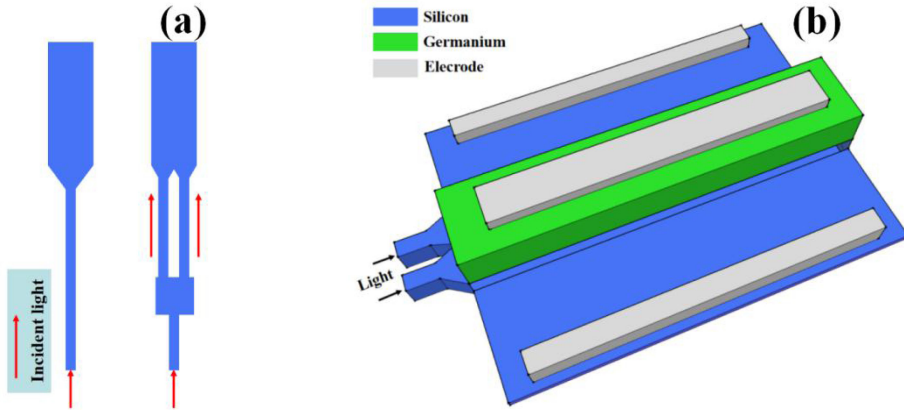


Fig. 1. (a) is the waveguide structure of single- and dual-injection devices, and (b) is the three-dimensional schematic of the Ge-on-Si positive-intrinsic-negative (PIN) photodetectors of dual-injection devices. The thickness of the silicon waveguide, germanium absorption and silicon slab layer are 220 nm, 500 nm and 60 nm respectively, the length of the slab is 1.5 μm . All of the heavily concentration are $1 \times 10^{20} \text{ cm}^{-3}$.

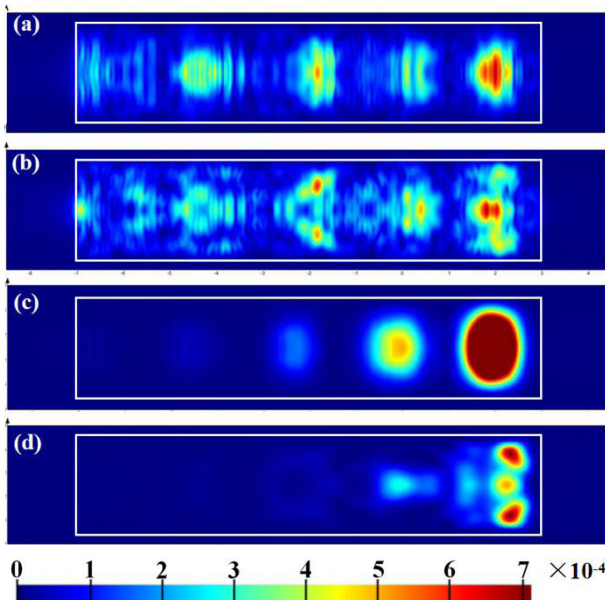


Fig. 2. Field distribution in the Ge absorption layer of single-injection photodetector @1550 nm (a), dual-injection photodetector @1550 nm (b), single-injection photodetector @1310 nm (c) and dual-injection photodetector @1310 nm (d) simulated by FDTD.

(FDTD) is shown in Fig. 2. FDTD uses the central difference quotient to replace the first-order partial derivative of the field quantity with respect to time and space. Through recurrence in the time domain, the wave propagation process is simulated to obtain the field distribution. Under the same incident optical power, the optical field distribution of the dual-injection structure is more extensive and uniform, the maximum optical field power of the dual-injection structure ($\sim 7.2 \times 10^{-4} \text{ w/m}^2$) is much smaller than single-injection structure ($\sim 8.7 \times 10^{-3} \text{ w/m}^2$) (as indicated by the scale in the simulation diagram), so its optical power distribution is more uniform. Because the dual-injection structure has two incident points, the light field distribution would be more dispersed. The light field gradually weakens from the center of the maximum to the surroundings. Since the dual-injection structure has more maximum points,

its light field distribution is more uniform. In addition, the interference and superposition of the two beams of light leads to a more uniform light field distribution. The 3 dB beam splitter in the dual-injection structure increases the light leakage, but the additional insertion loss is negligible.

In order to study the wavelength independent characteristic of the dual-injection structure, we also simulated the light field distribution with a input wavelength of 1310 nm, as shown in Fig. 2(c) and (d). The maximum value of the light field of the single-injection structure is about $9 \times 10^{-4} \text{ w/m}^2$, and the maximum value of the light field of the dual-injection structure is about $4.2 \times 10^{-4} \text{ w/m}^2$. The dual-injection structure also shows the extensive light field distribution comparing with the single-injection structure. Therefore, the purposed dual-injection structure photodetector can still make the light field intensity of the absorption region more uniform at the input wavelength of 1310 nm, thereby reducing the saturation effect and improving the performance of the device. At the 1310 nm wavelength, the light field is mainly distributed at the front end of the absorption zone since the absorption coefficient of germanium is higher at this wavelength ($7.8 \times 10^{-2} \text{ w/m}^2$), so most of the light field will be absorbed in a short absorption zone. The wavelength independency of the optimization effect benefited from the dual-injection structure is demonstrated in theoretically.

IV. PHOTOCURRENT

We simulated the photocurrent of the single- and dual-injection Ge-on-Si waveguide photodetectors as the rising incident light power at 1550 nm, the results are shown in Fig. 3. The curves of the photocurrent with the increasing incident optical power can be divided into three stages: linear region, nonlinear region and saturation region. In the first stage, the photocurrent increases linearly with the optical power, before the optical power incident to the single-injection photodetector reaches one. In the linear region stage, the responsivity of the photodetector is a constant value, which is the slope of the photocurrent curve. The responsivity of the single-injection photodetector is 1.291 A/W and 1.289 A/W for the dual-injection structure.

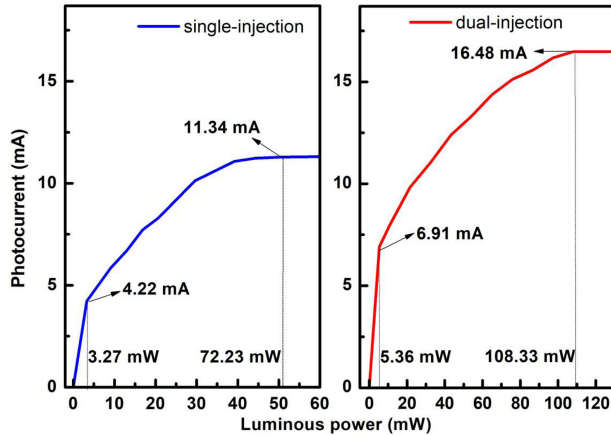


Fig. 3. The theoretically calculated photocurrent as a function of the input optical power at 1550 nm for both single- (a) and dual-injection (b) photodetectors.

When the incident light power increases to a certain value, the photogenerated carriers in the germanium absorption layer begin to be saturation, and this is the turning point of the photocurrent curve from linear to nonlinear. The second stage is the non-linear region. In this stage, the photocurrent still increases with the increasing optical power [18], but the saturation begins, the ascent rate gradually decreases. The third stage is the saturation stage, the photocurrent gets saturation (constant) and will not continue increasing anymore. These values of optical power refer to the total incident power from the optical waveguide.

In the first stage, single- and dual-incidence photodetectors have almost the same responsivity. There are mainly two reasons here. One is that more light leaks out of the optical waveguide in the dual-injection photodetector, which reduces its responsivity. On the other hand, the single-injection structure reduces the carrier collection efficiency due to the uneven carrier generation, which also reduces the responsivity. According to the unnoticeable difference in the responsivity of these two photodetectors at low optical power, the influence of the above two factors on the responsivity are small. After entering the second stage, the photo-generated carriers in some areas have reached saturation, and the saturation area increases as the incident light power increases. When the incident light power increases, the number of carriers generated in the saturated region will no longer increase and only the number of carriers generated in the unsaturated region can continue to contribute to photocurrent. Since the unsaturated region reduces gradually as the incident light power increases, the rising rate of its photocurrent slow down gradually as the incident optical power increases. In the third region, the photocurrent is a constant value. For the single-injection photodetector, the photocurrent reaches saturation (11.34 mA) when the incident light power is 72.23 mW. For the dual-injection one, the photocurrent reaches saturation (16.48 mA) when the incident light power is 108.33 mW. This is because the number of carriers generated in the entire optical field distribution area is saturated at this stage, and it will on longer increase with the optical power.

In the low incident power stage, the single- and dual-injection structure have almost the same responsivity, which is $\sim 1.29 \text{ A/W}$. When the incident light power exceeds 3.27 mW,

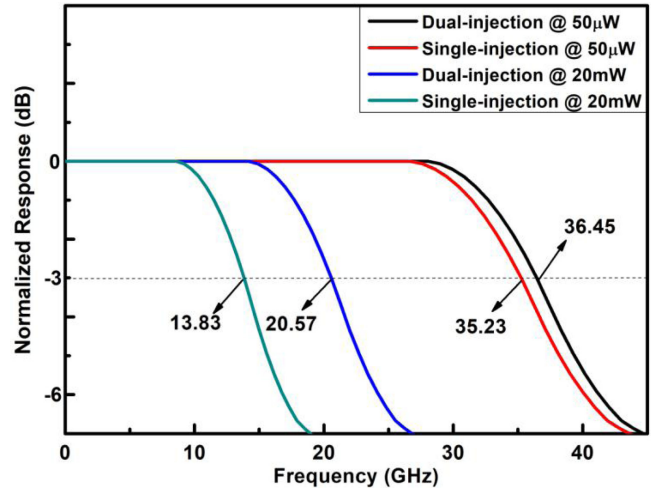


Fig. 4. Theoretical calculation of the bandwidth curve of the single- and dual-injection photodetectors under different optical powers (50 μW and 20 mW).

the difference of the responsivity between the single- and the dual-injection structure gradually increases. Under the high input optical power, the dual-injection photodetector shows obvious superiority, which is profited from the optical uniformity. Particularly, the saturated photocurrent of the dual-injection photodetector is 45.33% higher than that of the single-injection structure. When the incident light power reaches 108.33 mW, the responsivity of the dual-injection photodetector is higher than that of single-injection photodetector by 45.73%.

V. BANDWIDTH

Fig. 4 shows the theoretically calculated bandwidth characteristic curves of the single- and dual-injection photodetector. At low incident optical power (50 μW), the bandwidth of the dual-injection photodetector is 1.22 GHz larger than that of the single-injection structure. This is mainly caused by carrier-screening effect and diffusion effect. The applied electric field causes the photo-generated carriers (electron-hole pairs) moving directionally, in which electrons move to the cathode and holes move to the anode. The distribution of electrons and holes generates a built-in electric field, which weakens the applied electric field, thereby reducing the drift velocity of carriers. The higher light power produces more electron-hole pairs which lead to a more obvious carrier-screening effect. Since the light field distribution of the dual-injection structure is uniform, the local carrier concentration is smaller than that of the single-injection structure and could weaken the carrier-screening effect. In addition, the uneven distribution of photogenerated carriers in the single-injection structure also leads to the enhancement of the diffusion movement and weakens the directional movement [19]. When the incident light power is 20 mW, all of the bandwidth of these two structures decreases, but the single-injection configuration decreases faster. Under the incident power of 20 mW, the bandwidth of the dual-injection photodetector is 6.74 GHz larger than that of the single-injection photodetector. It is obvious that a uniform light field distribution can reduce the transit time of carriers, thereby effectively increase the bandwidth of the photodetector.

VI. CONCLUSION

We proposed a Ge-on-Si photodetector with a novel waveguide structure, the dual-injection structure. The photodetector with dual-injection waveguide structure can make the light field distribution in the germanium absorption layer of the photodetector more uniform, thereby effectively improving its performance. Compared with the traditional single-injection photodetector, the dual-injection photodetector has a larger saturated optical power and a larger bandwidth. The performance advantages are more obvious under a large incident optical power. Because of the larger light field area distribution, the saturated optical power of the dual-injection photodetector is 44.76% higher than that of the single-injection structure. Since the uniform light field can effectively weaken the carrier-screening effect, the dual-injection structure has a larger bandwidth. At low incident optical power (50 μW), the bandwidth of the dual-injection photodetector is 1.22 GHz larger than that of the single-injection. When the incident optical power is 20 mW, the bandwidth of the dual-injection photodetector is 6.74 GHz larger than that of the single-injection. The dark current of the photodetector mainly depends on the configuration of the active area [20], under the same active area configuration, our dual-injection photodetectors have the comparable dark current with single-injection devices in theory. The dual-injection structure improves the performance of the photodetector without increasing the complexity of the process or reducing the performance of other aspects of the device.

REFERENCES

- [1] J. Lin, H. Sepehrian, L. A. Rusch, and W. Shi, "CMOS-compatible silicon photonic IQ modulator for 84 gbaud 16QAM and 70 gbaud 32QAM," in *Proc. Opt. Fiber Commun. Conf. Expo.*, 2018, pp. 1–3.
- [2] S. B. Estrella *et al.*, "High-speed silicon photonic optical interconnects for cryogenic readout (Conference presentation)," in *Proc. Opt. Interconnects 20th Int. Soc. Opt. Photon.*, 2020, vol. 11286, Art. no. 112860B.
- [3] E. Sentieri *et al.*, "12.2 A 4-Channel 200Gb/s PAM-4 BiCMOS transceiver with silicon photonics front-ends for gigabit ethernet applications," in *Proc. IEEE Int. Solid-State Circuits Conf.*, 2020, pp. 210–212.
- [4] Y. Zhu *et al.*, "Hybrid plasmonic graphene modulator with buried silicon waveguide," *Opt. Commun.*, vol. 456, no. 9, 2020, Art. no. 124559.
- [5] D. Thomson *et al.*, "Roadmap on silicon photonics," *J. Opt.*, vol. 18, no. 7, 2016, Art. no. 073003.
- [6] M. Rakowski *et al.*, "45 nm CMOS-silicon photonics monolithic technology (45CLO) for next-generation, low power and high speed optical interconnects," in *Proc. Opt. Fiber Commun. Conf. Exhib.*, 2020, pp. 1–3.
- [7] X. Guan, R. Dube-Demers, W. Shi, and L. A. Rusch, "Heterogeneous optical access networks: Enabling low-latency 5G services with a silicon photonic smart edge," *J. Lightw. Technol.*, vol. 39, no. 8, pp. 2348–2357, Apr. 2021.
- [8] N. J. D. Martinez *et al.*, "Single photon detection in a waveguide-coupled Ge-on-Si lateral avalanche photodiode," *Opt. Exp.*, vol. 25, no. 14, 2017, pp. 16130–16139.
- [9] D. Seo, W.-B. Kwon, S. C. Kim, and C.-S. Park, "Frequency response estimation of 1.3 μm waveguide integrated vertical PIN type Ge-on-Si photodetector based on the analysis of fringing field in intrinsic region," *Curr. Opt. Photon.*, vol. 3, no. 6, pp. 510–515, 2019.
- [10] Z. Liu *et al.*, "Enhanced light trapping in Ge-on-Si-on-insulator photodetector by guided mode resonance effect," *J. Appl. Phys.*, vol. 124, no. 5, 2018, Art. no. 053101.
- [11] X. Zhang *et al.*, "Fabrication and performance of Ge-on-Si PIN photodetectors," in *Proc. Optoelectron. Devices Integration*, 2018, Art. no. 49.
- [12] J. Cui, T. Li, H. Chen, and W. Cui, "High-Performance microring resonator Ge-on-Si photodetectors by optimizing absorption layer length," *IEEE Photon. J.*, vol. 12, no. 4, Aug. 2020, Art. no. 6802208.
- [13] A. De Iacovo, A. Ballabio, J. Frigerio, L. Colace, and G. Isella, "Design and simulation of Ge-on-Si photodetectors with electrically tunable spectral response," *J. Lightw. Technol.*, vol. 37, no. 14, pp. 3517–3525, Jul. 2019.
- [14] Y. Zuo *et al.*, "Integrated high-power germanium photodetectors assisted by light field manipulation," *Opt. Lett.*, vol. 44, no. 13, pp. 3338–3341, 2019.
- [15] M. J. Byrd *et al.*, "Mode-evolution-based coupler for high saturation power Ge-on-Si photodetectors," *Opt. Lett.*, vol. 42, no. 4, pp. 851–854, 2017.
- [16] K. Shimomura, "Proposal of field-effect-type photodetector using field-screening effect in the absorption of light," *Japanese J. Appl. Phys.*, vol. 31, no. 12B, pp. L1757–L1759, 1992.
- [17] D. P. Singh and Y. P. Joshi, "Directional dependence of boundary-scattering mean free path of phonons in germanium and silicon," *Phys. Rev. B*, vol. 19, no. 6, pp. 3133–3136, 1979.
- [18] J. Cui *et al.*, "Optical saturation characteristics of dual- and single-injection Ge-on-Si photodetectors," *Chin. Opt. Lett.*, vol. 16, no. 7, Jul. 2018, Art. no. 072502.
- [19] T. Tanabe, H. Taniyama, and M. Notomi, "Carrier diffusion and recombination in photonic crystal nanocavity optical switches," *J. Lightw. Technol.*, vol. 26, no. 11, pp. 1396–1403, Jun. 2008.
- [20] M. Takenaka *et al.*, "Dark current reduction of Ge photodetector by GeO₂ surface passivation and gas-phase doping," *Opt. Exp.*, vol. 20, no. 8, pp. 8718–8725, 2012.